Physics Letters B 739 (2014) 56–61

Contents lists available at ScienceDirect

Physics Letters B

www.elsevier.com/locate/physletb

# Harmonic oscillator potential with a sextic anharmonicity in the prolate $\gamma$-rigid collective geometrical model

R. Budaca

*Horia Hulubei National Institute of Physics and Nuclear Engineering, RO-077125 Bucharest-Magurele, Romania*

ARTICLE INFO

*Article history:*
Received 8 August 2014
Received in revised form 26 September 2014
Accepted 10 October 2014
Available online 16 October 2014
Editor: J.-P. Blaizot

*Keywords:*
Collective states
Sextic oscillator

ABSTRACT

An analytical expression for the energy spectrum of the ground and $\beta$ bands was obtained through the JWKB approximation in the axially symmetric $\gamma$-rigid regime of the Bohr–Mottelson Hamiltonian with an oscillator potential and a sextic anharmonicity in the $\beta$ shape variable. Due to the scaling property of the problem, the resulting energy depends up to an overall multiplicative constant on a single parameter. Studying the behavior of the energy spectrum as a function of the free parameter, one establishes the present model's place among other prolate $\gamma$-rigid models and in the more general extent of collective solutions. The agreement with experiment is achieved through model fits for few nuclei.



## 1. Introduction

Fixing the $\gamma$ shape variable to 0° in the Bohr–Mottelson classical model [1] leads to a whole new space of collective phenomena described in terms of only three variables, i.e. two Euler angles and the $\beta$ shape variable. This particular construction facilitates the exact separation of angular variables from the $\beta$ variable. The first venture into this subject was made in Ref. [2], where the authors proposed a parameter-free model based on the square well potential in $\beta$ variable. Due to the choice of the potential and the closeness to the $X(5)$ predictions [3], the model was named $X(3)$. Although the square well shape is a suitable approximation for the collective potential [4,5], a more natural choice is the harmonic oscillator amended with higher order anharmonic terms. A special attention in this sense is deserved by the sextic oscillator which not only simulates the square well but can also provide a deformed minimum. Besides, it is also the lowest order polynomial potential which is quasi-exactly solvable [6]. However, analytical solutions are available only for a family of potentials, whose coefficients satisfy certain relations between them and the angular momentum of the centrifugal term. Due to the condition of a constant potential, the exact solutions cannot be achieved in the prolate $\gamma$-rigid case as it happens in the $\gamma$ stable [7,8] and $\gamma$ unstable [9,10] realizations.

In this paper I propose an approximate analytical formula for the energy spectrum of a prolate $\gamma$-rigid collective Hamiltonian with a harmonic oscillator potential corrected by a sextic term, which is based on the fourth order approximation made on the JWKB quantization rule [11]. The shape of such a potential resembles a smoothed out square well, the resulting formalism being considered thus as a $X(3)$ derivative. It is found that the corresponding energy spectrum depends up to a factor on a single free parameter, which when vanishing leads to a parameter-free $X(3)$-$\beta^6$ model. On the other hand, the adopted approximation has a finite convergence radius which is determined in respect with exact numerical energies. The experimental realization of the model is found in $^{102}$Pd, $^{150}$Sm and $^{222}$Th nuclei, while $^{176}$Pt appears to be a suitable candidate for $X(3)$-$\beta^6$.

## 2. Prolate $\gamma$-rigid collective Hamiltonian with a sextic anharmonicity

The Hamiltonian associated with a prolate $\gamma$-rigid nucleus is [2,12]:

$$H=-\frac{\hbar^2}{2B}\left[\frac{1}{\beta^2}\frac{\partial}{\partial\beta}\beta^2\frac{\partial}{\partial\beta}-\frac{\hat{\mathbf{I}}^2}{3\hbar^2\beta^2}\right]+U(\beta), \tag{2.1}$$

where $\hat{\mathbf{I}}$ is the angular momentum operator from the intrinsic frame of reference, while $B$ is the mass parameter. The Schrödinger equation associated to such a Hamiltonian is solved by separating the $\beta$ variable from the angular ones which is achieved through the factorization:

$$\Psi(\beta,\theta_1,\theta_2)=F(\beta)Y_{IM}(\theta_1,\theta_2), \tag{2.2}$$

*E-mail address:* rbudaca@theory.nipne.ro.

http://dx.doi.org/10.1016/j.physletb.2014.10.031

where the angular factor state is a spherical harmonic function and has the property:

$$\hat{\mathbf{I}}^2 Y_{IM}(\theta_1,\theta_2) = I(I+1)\hbar^2 Y_{IM}(\theta_1,\theta_2). \tag{2.3}$$

With this, the Schrödinger equation is reduced to a second order differential equation in variable $\beta$:

$$\left[\frac{1}{\beta^2}\frac{d}{d\beta}\beta^2\frac{d}{d\beta} - \frac{I(I+1)}{3\beta^2} + \frac{2B}{\hbar^2}\big(E-U(\beta)\big)\right]F(\beta) = 0. \tag{2.4}$$

Making the change of function $F(\beta) = \frac{f(\beta)}{\beta}$ and the denotations $\varepsilon = BE/\hbar^2$, $u(\beta) = BU(\beta)/\hbar^2$, one obtains an equation which resembles the radial Schrödinger equation for a three-dimensional isotropic potential $u(\beta)$:

$$\left[\frac{d^2}{d\beta^2} - \frac{I(I+1)}{3\beta^2} + 2\big(\varepsilon - u(\beta)\big)\right]f(\beta) = 0. \tag{2.5}$$

The potential is chosen to be of the following form:

$$u(\beta) = \frac{1}{2}\alpha_1\beta^2 + \alpha_2\beta^6, \quad \alpha_1 \geqslant 0,\ \alpha_2 > 0. \tag{2.6}$$

The eigenvalue problem for such a potential has the following scaling property:

$$\varepsilon(\alpha_1,\alpha_2) = \alpha_2^{\frac{1}{4}}\varepsilon(\lambda,1) = \alpha_2^{\frac{1}{4}}W(\lambda), \quad \lambda = \alpha_1\alpha_2^{-\frac{1}{2}}, \tag{2.7}$$

which follows from the change of variable $\beta' = \alpha_2^{\frac{1}{8}}\beta$ in the differential equation (2.5). The problem is then reduced to solving the radial Schrödinger equation with a modified centrifugal term for the scaled potential:

$$\tilde{u}(\beta') = \frac{1}{2}\lambda\beta'^2 + \beta'^6, \quad \lambda \geqslant 0. \tag{2.8}$$

The Schrödinger equation for such a potential is not exactly solvable, thus an approximate method is required. For this, one adapts the method from Ref. [11] for finding the eigenvalue $W$, to the present case of the modified centrifugal term. Following the procedure of Ref. [11] one can write the eigenvalue $W$ as function of $\lambda$, $n$ – the $\beta$ vibration quantum number and the intrinsic angular momentum $I$, as follows:

$$W_{nI}(\lambda) = (N_{nI})^{\frac{3}{2}}\sum_{k=0}^{5} G_k(\lambda,I)(N_{nI})^{-k}, \tag{2.9}$$

where

$$N_{nI} = 2\sqrt{2}a\left[2n+1+\frac{1}{2}\sqrt{1+\frac{4I(I+1)}{3}}\right], \tag{2.10}$$

with the functions $G_k(\lambda,I)$ given in Appendix A where the constant $a$ is also defined.

The energy spectrum of a nucleus described by the Hamiltonian (2.1) with a potential defined by Eq. (2.8) is then determined by the following expression:

$$E_{nI} = \frac{\hbar^2}{B}\alpha_2^{\frac{1}{4}}\big[W_{nI}(\lambda) - W_{00}(\lambda)\big]. \tag{2.11}$$

## 3. Model characteristics

The energy levels of the ground state band ($n=0$), as well as of the $\beta$ vibrational bands ($n>0$) defined by Eq. (2.11) depend on a single parameter, i.e. $\lambda$, up to a multiplying constant. Before analyzing the evolution of the energy spectrum as function of $\lambda$ it is necessary to establish the limit where the adopted approximation starts to diverge from the exact numerical solutions. Taking into account the fact that the accuracy of the JWKB based eigenvalues is improving with the increasing of the quantum numbers [13], one will limit the comparison only to the ground state which is the same as in the case of the usual centrifugal term. There are very few numerical estimates of the eigenvalues corresponding to this particular form of the potential and only for the one-dimensional case. However, making a correspondence between the associated quantum numbers, one finds that the ground state in the three-dimensional case is equivalent to the first excited state from the one-dimensional case. In Refs. [14,15] the corresponding eigenvalues are computed for some selected values of the parameter $\lambda$ which are linearly interpolated in Fig. 1, in order to simulate a continuous dependence. Comparing the resulting curve with that given by the present model visualized on the same graph one ascertains that the convergence radius of our approximate formulas is about $\lambda_c = 10$.

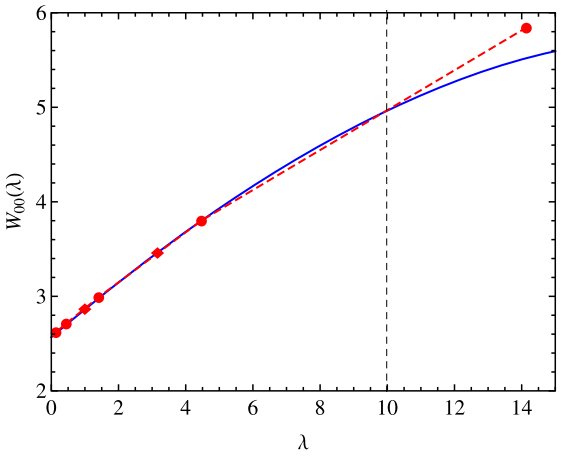


**Fig. 1.** Theoretical ground state energy $W_{00}$ as function of $\lambda$ represented by the solid line is compared to few exact eigenvalues taken from [14] (circles) and [15] (diamonds) which are interpolated by straight dashed lines between them.

The evolution of the energy spectrum normalized to the first excited state and comprising the ground and two excited $\beta$ bands as function of $\lambda$ in the interval $[0,10]$ is depicted in Fig. 2. From there one can see that the low lying states from different bands become almost degenerate in the second half of the considered interval, becoming more distinct at high angular momenta. Also as $\lambda$ goes from 0 to 10 the states $I_1^+$ and $(I-4k)_k^+ (k>1)$ change their order and at some point intersect each other. Also for each value of $\lambda$ the spectra of the considered bands are almost identical being differentiated only by their relative positions, i.e. bandheads.

The convergence radius $\lambda_c = 10$ does not in any way limit the model's applicability. Indeed, as the scaled variable $\beta'$ is under unity in the region of interest, a higher value for $\lambda$ would bring the potential into the harmonic limit. This can be seen from Fig. 3, where the line corresponding to $\lambda = 10$ is very close to the $X(3)$-$\beta^2$ predictions for the low spin states. Moreover, the states of different bands are almost degenerated in the spectrum of $\lambda = 10$ (see Fig. 2) which is consistent with the $X(3)$-$\beta^2$ behavior. In both graphs of Fig. 3 representing the ground and first $\beta$ bands, the spectra covered by the present model are situated in the middle between the predictions of the $X(3)$ [2] and $X(3)$-$\beta^2$ limiting models, more closer to the last in the $\beta$ band case. Additionally, it seems that the model extension also covers the spectrum of the $X(3)$-$\beta^4$ model [12] with a different distribution of states. The spectra in the acting interval vary uniformly equidistant from $\lambda = 0$ to $\lambda_c = 10$. It is worth to mention that for $\lambda = 0$ one obtains a parameter-free model denoted $X(3)$-$\beta^6$ due to the already es-

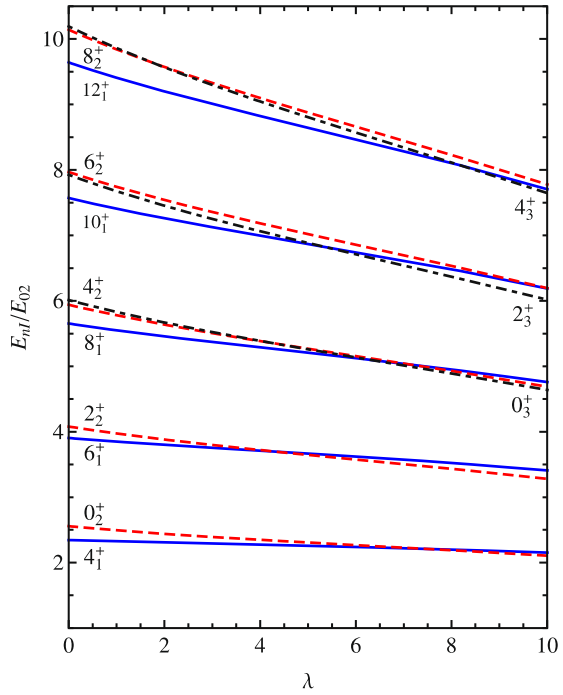


**Fig. 2.** Theoretical energy spectrum normalized to the energy of the state $2_1^+$ given as function of $\lambda$. The full, dashed and dot-dashed lines correspond to the ground, first and respectively second excited $\beta$ bands.

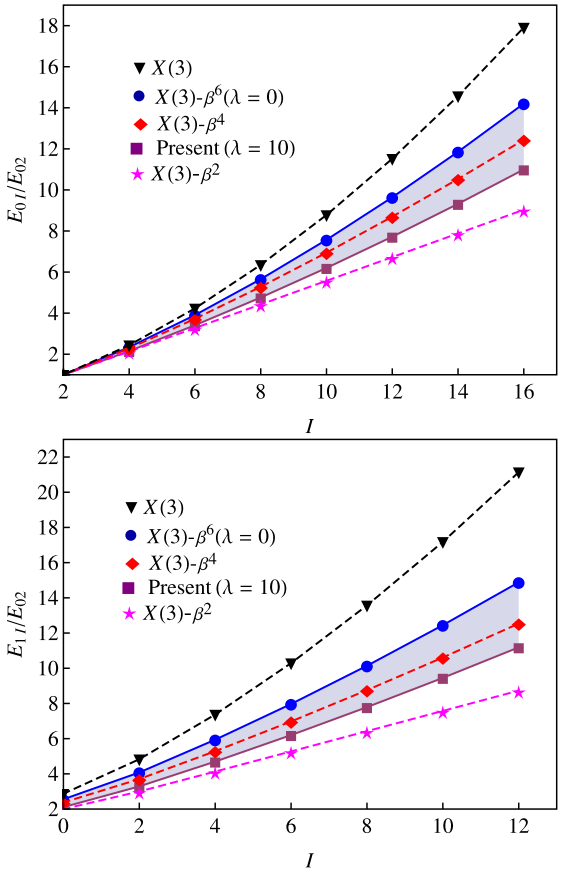


**Fig. 3.** Ground band (top) and the first $\beta$ band (bottom) theoretical energy spectra normalized to the first excited state energy are given as a function of angular momentum for $\lambda = 0$ and $\lambda = 10$ which enclose the existence region of the model (gray area). The $X(3)$ [2], $X(3)$-$\beta^2$ and $X(3)$-$\beta^4$ [12] predictions are also shown for comparison.

**Table 1**
Few energy levels of the $X(3)$-$\beta^6$ model, normalized to the $2_1^+$ excited state energy.

| $I$ | $E_{0I}/E_{02}$ | $E_{1I}/E_{02}$ | $E_{2I}/E_{02}$ |
|---|---|---|---|
| 0 | 0.000 | 2.556 | 6.013 |
| 2 | 1.000 | 4.080 | 7.925 |
| 4 | 2.343 | 5.941 | 10.193 |
| 6 | 3.905 | 7.968 | 12.606 |
| 8 | 5.654 | 10.141 | 15.141 |
| 10 | 7.571 | 12.449 | 17.791 |
| 12 | 9.642 | 14.884 | 20.551 |

tablished nomenclature [2,12] and whose normalized spectrum is given separately in Table 1. Summing up, the model's acting space given in terms of the ratio $R_{4/2} = E(4_1^+)/E(2_1^+)$ is enclosed between 2.343 and 2.154, while the bandhead of the first $\beta$ band denoted $R_{0/2}$ lies between 2.556 and 2.109 with the limits corresponding to the $X(3)$-$\beta^6$ model with $\lambda = 0$ and respectively the cutoff value $\lambda_c$.

Besides the conclusions drawn from Fig. 3, it is desirable to place the present results in a wider context of collective models. This is done in Table 2, where the signature ratios $R_{4/2}$ and $R_{0/2}$ of the proposed formalism are compared with those provided by other models with similar values. The parameter-free dynamical symmetries included in comparison are schematically discussed in Ref. [5] and reviewed in more detail along with other analytical solutions in Ref. [16]. There are other models which fall in the same criteria for comparison, but not listed due to their complex structure and greater number of adjustable parameters. The $\gamma$ unstable cases of the Morse potential [19], Davidson [17] and Kratzer [18] potentials amended with a deformation dependent mass term and their soft triaxial solutions [20], are a few of them. Also one cannot omit the recently developed Algebraic Collective Model [21–23] which provides accurate and rapidly converging numerical solutions of the collective Hamiltonian for many different potentials. From Table 2 one can see that concerning the existence intervals, the $X(3)$ related models are close to the triaxial rigid and $\gamma$-unstable solutions. In particular, the $E(5)$-$\beta^{2n}$ models seem to be the closest ones, even with neighboring candidates like $^{100}$Pd and $^{102}$Pd. Moreover, in Ref. [27] it was shown that the critical point symmetry of the $U(5) \leftrightarrow O(6)$ shape phase transition should be the $E(5)$-$\beta^4$ model instead of $E(5)$. This claim enforces the importance for the study of the polynomial potentials.

The model proposed provides a polynomial formula for the energy, but unfortunately no information on the wave functions which are essential for computing electromagnetic transitions. Despite this shortcoming, the usefulness of the model resides in the continuous description of the energy spectrum as function of a single parameter. Knowing the value of the free parameter for a certain nucleus, one can therefore compute numerically some transition probabilities which is not an easy task and it is not the scope of the present letter.

## 4. Experimental realization

The experimental realization of the model was found to occur in $^{102}$Pd, $^{150}$Sm, $^{176}$Pt and $^{222}$Th, whose model fits provide the best agreement. In order to obtain a quantitative measure of the agreement, one fitted the absolute experimental spectra with the energy function (2.11), obtaining thus the multiplying constant $\hbar^2\alpha_2^{1/4}/B$ and the parameter $\lambda$. The results of the fits are given in Fig. 4, while the corresponding parameters are listed in Table 3. Although the energy spectrum and the shape of the potential are completely determined only by $\lambda$, the unscaled potential (2.6) can be recovered. Indeed, equating the expression for the ground state

**Table 2**
Comparison of the present model with other relevant solutions in terms of the application range defined only by $R_{4/2}$ and $R_{0/2}$ signatures. i.s.w. stands for infinite square well. Apart from the original reference, the candidate nuclei are also complemented from Refs. [4,5]. Only the nuclei with a $\beta$ band were considered as candidates for the $X(3)$-$\beta^{2n}$ models. The upper signature ratios of the last three solutions correspond to the $O(6)$ limit [31].

| Model ref. | $v(\beta)$ | $\gamma$ or $v(\gamma)$ | $R_{4/2}$ | $R_{0/2}$ | Candidates |
|---|---|---|---|---|---|
| $X(3)$-$\beta^2$ [12] | $\beta^2$ | 0° | 2.13 | 2.00 | – |
| $X(3)$-$\beta^4$ [12] | $\beta^4$ | 0° | 2.29 | 2.37 | $^{154}$Dy |
| [12] | $\frac{1}{2}\lambda\beta^2+\beta^4$ | 0° | 2.00–2.29 | 1.81–2.37 | $^{100}$Mo, $^{152}$Gd |
| $X(3)$-$\beta^6$ | $\beta^6$ | 0° | 2.34 | 2.56 | $^{102}$Pd, $^{176}$Pt |
| Present | $\frac{1}{2}\lambda\beta^2+\beta^6$ | 0° | 2.15–2.34 | 2.11–2.56 | $^{102}$Pd, $^{150}$Sm |
| $X(3)$ [2] | i.s.w. | 0° | 2.44 | 2.87 | $^{172}$Os, $^{186}$Pt |
| $Z(4)$-$\beta^2$ [24] | $\beta^2$ | 30° | 2.00 | 3.00 | – |
| $Z(4)$ [25] | i.s.w. | 30° | 2.23 | 2.95 | $^{128,130,132}$Xe |
| $U(5)$ [26] | $\beta^2$ | unstable | 2.00 | 2.00 | Many |
| $E(5)$-$\beta^4$ [27,28] | $\beta^4$ | unstable | 2.09 | 2.39 | $^{100}$Pd |
| $E(5)$-$\beta^6$ [29] | $\beta^6$ | unstable | 2.14 | 2.62 | $^{98}$Ru |
| $E(5)$-$\beta^8$ [29] | $\beta^8$ | unstable | 2.16 | 2.76 | – |
| $E(5)$ [30] | i.s.w. | unstable | 2.19 | 3.03 | $^{104}$Ru, $^{106,108}$Cd $^{102}$Pd, $^{128}$Xe, $^{134}$Ba |
| [31] | $(\beta-\beta_0)^2$ | unstable | 2.00–2.50 | 2.00–$\infty$ | Many |
| [32] | Davidson | unstable | 2.00–2.50 | 2.00–$\infty$ | – |
| [33] | Kratzer | unstable | 1.35–2.50 | 1.00–$\infty$ | – |

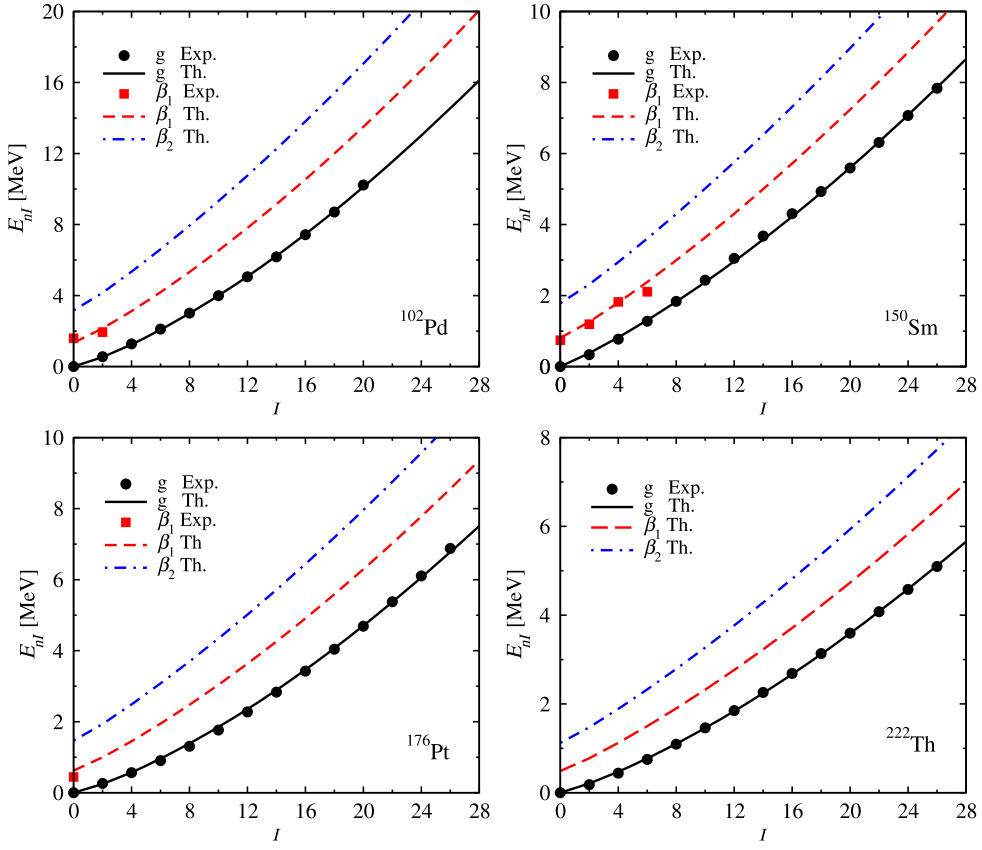


**Fig. 4.** Theoretical results for ground, first and second excited $\beta$ bands energies are compared with the available experimental data for $^{102}$Pd [35], $^{150}$Sm [36], $^{176}$Pt [37] and $^{222}$Th [38].

of the $\beta^2$ average derived from the hypervirial relations [34] using Hellmann–Feynman theorem,

$$\langle n,I|\beta^2|n,I\rangle = 2\alpha_2^{-\frac{1}{4}}\frac{\partial W_{nI}}{\partial\lambda}, \tag{4.12}$$

with a tabulated value of the quadrupole deformation one obtains a determining equation for $\alpha_1$. Finally, $\alpha_2$ is extracted from $\lambda=\alpha_1\alpha_2^{-\frac{1}{2}}$. The resulting values for the considered nuclei are listed in Table 3 together with all other ingredients, while the corresponding potentials are plotted as function of $\beta$ in Fig. 5.

The results of Table 3 reveal that $^{150}$Sm and $^{176}$Pt are situated at the limits of the present model, being characterized by $\lambda=9.6$ and respectively $\lambda=0$ which marks the $X(3)$-$\beta^6$ model presented in the last section. Apart from $^{176}$Pt, another candidate for $X(3)$-$\beta^6$

**Table 3**
The parameters obtained from the fits visualized in Fig. 4 corroborated with the tabulated quadrupole deformations $\beta_2$ [39] used for determining $\alpha_1$ and $\alpha_2$. The quantity $\partial W_{00}/\partial\lambda$ essential for finding $\alpha_2$, the number of fitted states and the corresponding deviation $\sigma = \sqrt{\sum_i^N (E_i^{\rm exp} - E_i^{Th})^2/N}$ are also listed.

| Nucleus | $\beta_2$ | $\lambda$ | $\frac{\partial W_{00}}{\partial\lambda}$ | $\alpha_1$ | $\alpha_2$ | $\hbar^2/B$ [keV] | Nr. states | $\sigma$ [keV] |
|---|---|---|---|---|---|---|---|---|
| $^{102}$Pd | 0.133 | 0.5130 | 0.29474 | 569.7 | $1.2333 \cdot 10^6$ | 6.3188 | 12 | 102.292 |
| $^{150}$Sm | 0.206 | 9.6001 | 0.17569 | 658.2 | $0.0047 \cdot 10^6$ | 12.1657 | 17 | 83.123 |
| $^{176}$Pt | 0.171 | 0 | 0.29923 | 0 | $0.1755 \cdot 10^6$ | 4.8266 | 14 | 72.920 |
| $^{222}$Th | 0.111 | 3.7289 | 0.25873 | 6577.4 | $3.1113 \cdot 10^6$ | 1.6871 | 13 | 15.945 |

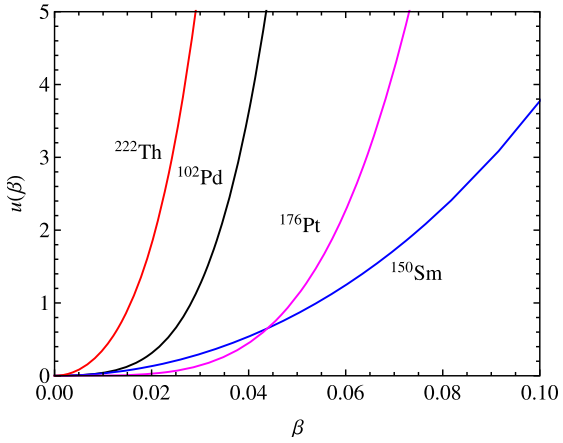


**Fig. 5.** Potential (2.6) in the origin region as function of $\beta$ for the considered nuclei with coefficients $\alpha_1$ and $\alpha_2$ listed in Table 3.

could be considered the $^{102}$Pd nucleus, for which one obtains a small value for $\lambda$. This nucleus was also treated in Refs. [17–19] where only $R_{4/2}$, and the $\beta$ and $\gamma$ bandheads were fitted. The best agreement with experiment is obtained with Morse potential [19], where although $R_{4/2}$ is very well reproduced the $R_{0/2}$ is overestimated with poorer accord with experiment than in the present calculations. The three nuclei with $\lambda > 0$ share a common feature which is the number of nucleons (three) above the shell closure at the magic numbers $N = 50, 82$ and respectively $N = 126$. It is also interesting that their lighter neighbors were successfully described with a quartic anharmonicity [12]. Exception is the $X(3)$-$\beta^6$ nucleus $^{176}$Pt, which seems to be a critical one for its isotopic chain, given the fact that it has the smallest value of $R_{4/2}$ ratio. Moreover, $\lambda = 0$ from Fig. 5 corresponds to the flattest potential in the framework of the present model which is a determining characteristic for a critical point. Although for nucleus $^{222}$Th, there are no experimental data available for the $\beta$ bands, it is certainly worth mentioning because of the precise reproduction of the ground band states up to $I = 26$.

## 5. Outlook

Based on higher order JWKB approximation, an analytical formula is derived for the energy spectrum of the prolate $\gamma$-rigid Bohr–Mottelson Hamiltonian with an oscillator potential and a sextic anharmonicity in $\beta$ shape variable. The energy formula depends up to an overall factor on a single free parameter which is bounded by the convergence radius $\lambda_c = 10$ of the adopted approximation. The acting space of the model is then restricted to the interval $[0, \lambda_c]$ which put in terms of the ratios $R_{4/2}$ and $R_{0/2}$ lies between $[2.343, 2.154]$ and $[2.556, 2.109]$, respectively. The upper limit corresponds to $\lambda = 0$ which is associated to the free parameter model $X(3)$-$\beta^6$, while the lower limit is close to the $X(3)$-$\beta^2$ predictions. The spectra described by the present model decrease uniformly in energy as the free parameter goes from 0 to $\lambda_c$ and are placed in the middle between the $X(3)$ and $X(3)$-$\beta^2$ boundary models covering also the spectrum provided by $X(3)$-$\beta^4$. It was also pointed out that its application range overlaps with that of the $E(5)$-$\beta^{2n}$ models. The model is experimentally realized for $^{102}$Pd, $^{150}$Sm, $^{176}$Pt and $^{222}$Th nuclei for which were performed quantitative fits, revealing the nucleus $^{176}$Pt as a suitable candidate for the $X(3)$-$\beta^6$ model.

Before closing, it is worth to note that the present approximate formula can be easily translated to the case of four- and five-dimensional Bohr–Mottelson Hamiltonians with a similar separated potential for the $\beta$ shape variable.

## Appendix A

The functions $G_k(\lambda, I)$ defining the energy $W_{nI}(\lambda)$ are taken from [11] and adjusted to the present physical problem acquire the following expressions:

$$G_0 = 1, \qquad G_1 = \frac{\lambda a}{2},$$

$$G_2 = \frac{b}{12}\big[5 - 4I(I+1)\big] + \frac{\lambda^2}{24}\big(a^2 - b\big),$$

$$G_3 = \frac{\lambda}{144}\big[3 - 10ab + 4(1 + 2ab)I(I+1)\big] - \frac{\lambda^3}{864}\big(1 - 6ab + 2a^3\big),$$

$$G_4 = -\frac{1}{288}\Big\{b^2\big[25 - 40I(I+1) + 16I^2(I+1)^2\big] - \lambda^2\big[5b^2 + 5a^2b - 3a - 4\big(a + b^2 + a^2b\big) \times I(I+1)\big] - \frac{\lambda^4}{12}\big(2a - 3b^2 - 6a^2b + a^4\big)\Big\},$$

$$G_5 = \frac{5}{1728}\Big\{\lambda b\big[24 + 25ab + 8(4 - 5ab)I(I+1) + 16abI^2(I+1)^2\big] + \frac{\lambda^3}{6}\big[9a^2 - 10ab\big(3b + a^2\big) - 8b + 4a\big(3a + 6b^2 + 2a^2b\big)I(I+1)\big] + \frac{\lambda^5}{12}\left(2a^3b - a^2 + 3ab^2 - \frac{a^5}{5}\right)\Big\},$$

where

$$a = \frac{\pi\,\Gamma(\frac{2}{3})}{\Gamma(\frac{1}{6})\Gamma(\frac{1}{2})}, \qquad b = \frac{\Gamma(\frac{5}{6})\Gamma(\frac{2}{3})}{\Gamma(\frac{1}{6})\Gamma(\frac{4}{3})}. \tag{4.13}$$

## References

[1] A. Bohr, B. Mottelson, Mat. Fys. Medd. Dan. Vid. Selsk. 27 (1953) 16.
[2] D. Bonnatsos, D. Lenis, D. Petrellis, P.A. Terziev, I. Yigitoglu, Phys. Lett. B 632 (2006) 238.
[3] F. Iachello, Phys. Rev. Lett. 87 (2001) 052502.
[4] P. Cejnar, J. Jolie, R.F. Casten, Rev. Mod. Phys. 82 (2010) 2155.

[5] R.F. Casten, Nat. Phys. 2 (2006) 811.
[6] A.G. Ushveridze, Quasi-Exactly Solvable Models in Quantum Mechanics, Institute of Physics Publishing, Bristol and Philadelphia, 1993.
[7] A.A. Raduta, P. Buganu, Phys. Rev. C 83 (2011) 034313.
[8] A.A. Raduta, P. Buganu, J. Phys. G, Nucl. Part. Phys. 40 (2013) 025108.
[9] G. Levai, J.M. Arias, Phys. Rev. C 69 (2004) 014304.
[10] G. Levai, J.M. Arias, Phys. Rev. C 81 (2010) 044304.
[11] S.S. Vasan, M. Seetharaman, L. Sushama, Pramana J. Phys. 40 (1993) 177.
[12] R. Budaca, Eur. Phys. J. A 50 (2014) 87.
[13] F.T. Hioe, Don Macmillen, E.W. Montroll, Phys. Rep. 43 (1978) 305.
[14] K. Banerjee, Proc. R. Soc. Lond. A 364 (1978) 255.
[15] H. Meissner, E. Otto Steinborn, Phys. Rev. A 56 (1997) 1189.
[16] L. Fortunato, Eur. Phys. J. A 26 (2005) 1.
[17] D. Bonatsos, P.E. Georgoudis, D. Lenis, N. Minkov, C. Quesne, Phys. Rev. C 83 (2011) 044321.
[18] D. Bonatsos, P.E. Georgoudis, N. Minkov, D. Petrellis, C. Quesne, Phys. Rev. C 88 (2013) 034316.
[19] I. Boztosun, D. Bonatsos, I. Inci, Phys. Rev. C 77 (2008) 044302.
[20] L. Fortunato, S. De Baerdemacker, K. Heyde, Phys. Rev. C 74 (2006) 014310.
[21] D.J. Rowe, Nucl. Phys. A 735 (2004) 372.
[22] D.J. Rowe, P.S. Turner, Nucl. Phys. A 753 (2005) 94.
[23] D.J. Rowe, T.A. Welsh, M.A. Caprio, Phys. Rev. C 79 (2009) 054304.
[24] E.A. McCutchan, D. Bonatsos, N.V. Zamfir, R.F. Casten, Phys. Rev. C 76 (2007) 024306.
[25] D. Bonatsos, D. Lenis, D. Petrellis, P.A. Terziev, I. Yigitoglu, Phys. Lett. B 621 (2005) 102.
[26] A. Bohr, Mat. Fys. Medd. Dan. Vid. Selsk. 26 (1952) 14.
[27] J.M. Arias, et al., Phys. Rev. C 68 (2003) 041302(R).
[28] O.K. Vorov, V.G. Zelevinsky, Nucl. Phys. A 439 (1985) 207.
[29] D. Bonatsos, D. Lenis, N. Minkov, P.P. Raychev, P.A. Terziev, Phys. Rev. C 69 (2004) 044316.
[30] F. Iachello, Phys. Rev. Lett. 85 (2000) 3580.
[31] L. Wilets, M. Jean, Phys. Rev. 102 (1956) 788.
[32] J.P. Elliott, et al., Phys. Lett. B 169 (1986) 309.
[33] L. Fortunato, A. Vitturi, J. Phys. G, Nucl. Part. Phys. 29 (2003) 1341.
[34] D.E. Hughes, J. Phys. B, At. Mol. Opt. Phys. 10 (1977) 3167.
[35] D. De Frenne, Nucl. Data Sheets 110 (2009) 1745.
[36] S.K. Basu, A.A. Sonzogni, Nucl. Data Sheets 114 (2013) 435.
[37] M.S. Basunia, Nucl. Data Sheets 107 (2006) 791.
[38] S. Singh, A.K. Jain, J.K. Tuli, Nucl. Data Sheets 112 (2011) 2851.
[39] P. Moller, J.R. Nix, W.D. Meyers, W.J. Swiatecki, At. Data Nucl. Data Tables 59 (1995) 185.